

Phase Transformation, Micro-structure, Crystal Growth Kinetics of Fe³⁺-Doped Titanium Dioxide Prepared by TiCl₄ Hydrolyzation

MIAO SHUI*, YUE SONG, QINGCHUN WANG and YUANLONG REN

Faculty of Materials Science and Chemical Engineering, The State Key Laboratory Base of Novel Functional Materials and Preparation Science, Ningbo-315211, P.R. China
Fax: (86)(574)87600734; Tel: (86)(574)87600147; E-mail: shuimiao@nbu.edu.cn

Titania based ceramics are promising materials for environmental sensors, high efficiency photocatalyst. Ion doping is an effective method to improve the properties by modifying their micro-structure and phase composition. In this study, pure TiO₂, co-precipitation Fe³⁺-doped TiO₂ and step-precipitation Fe³⁺-doped TiO₂ are synthesized by means of TiCl₄ hydrolyzation. Thermal analysis, TEM and X-ray diffraction are used to characterize the Fe³⁺-doped TiO₂ powder. Micro-strain, crystallite size, phase content and cell parameters are calculated according to rietveld refinement software GSAS. The interaction mechanism of Fe³⁺ in crystal lattice of titanium dioxide and the crystal growth kinetics Fe³⁺-doped TiO₂ are intensively investigated.

Key Words: Titanium dioxide, Rietveld, General structure analysis system, Fe³⁺ doping, X-ray.

INTRODUCTION

In recent years, the preparation and characterization of titanium oxide based composites have attracted much interest due to their unique properties and potential applications in catalyst¹/photo-catalyst², catalyst carrier³, sensors⁴ for being sensitive to a variety of gases such as carbon monoxide, humidity and hydrogen, solar cells^{5,6}, energy storage⁷ and electronic devices⁸.

It has been demonstrated that the physical and chemical properties of TiO₂ based ceramics and hence their potential applications depend strongly on their crystalline structure, morphology, crystallite size, particle size/size distribution, phase composition and surface characteristics⁹. Therefore, accurate control to the micro-structure will help to improve the application performance. Fortunately, these requirements can be tailored in the preparation by element doping, multi-phase composite and varying sintering temperature. Mardare *et al.*¹⁰ noticed that in Fe³⁺-doped TiO₂ films deposited on indium tin oxide substrates, a combined effect of substrate and doping occurs, leading to the increase of anatase phase and thus to better super-hydrophilic properties and higher photocatalytic efficiency. Zhang¹¹ observed an apparent change of preferred orientation and mixed titanium oxidation states in the case of Fe-doped TiO₂ films. The absorption edge of Fe-doped TiO₂ film shifts toward longer wavelength and the films with appropriate Fe³⁺ concentration show

better photocatalytic activity than pure TiO₂ films. Hazra and Basu¹² prepared Al³⁺-doped porous titania thin films by thermal oxidation of titanium substrates; the sensor shows appreciably high sensitivity and fast response to hydrogen.

Fe³⁺ ions are good candidates for modifying the sintering process and improving the properties of functional ceramics. Comprehensive studies on thermal behaviour, micro-structure, phase transformation and crystal growth kinetics of nano-scale Fe³⁺-doped TiO₂ are rarely reported. In this paper, the phase transformation, crystal growth kinetics and thermal stability of Fe-doped titanium dioxide prepared by TiCl₄ hydrolyzation are studied. Rietveld refinement method is applied here to calculate the micro-structure parameters of the Fe-doped titanium dioxide.

EXPERIMENTAL

Preparation of Fe-doped titanium dioxide by TiCl₄ hydrolyzation

Co-precipitation: 20 mL of TiCl₄ (AR) was extracted from the bottle and quickly injected into a flask with 200 mL of 30 % HCl solution under strong stirring. At the same time, calculated amount of 5 % of Fe(NO₃)₃ solution was added dropwise until the solution in the flask turned mauve but still transparent. Then adjust the pH level of the system to 6-7 with ammonia. Large amount of precipitates were obtained. They were filtrated and washed by distilled water for several times until no Cl⁻ can be detected by 0.1 M AgNO₃. The filter cakes were dried at constant temperature for 24 h and then sieved through 80 mesh screen. The as-prepared samples were calcinated for 3 h at 110, 250, 400, 500, 600 and 700 °C, respectively.

Step precipitation process: 20 mL of TiCl₄ (AR) was injected quickly into a flask containing 200 mL of 30 % HCl solution under strong stirring. Adjust the pH value of the solution to 6-7 with ammonia. Titanium hydroxide precipitated quickly. Then 5 % of Fe(NO₃)₃ solution was added drop-wise under strong stirring. The solution was then filtered and washed for several times until no Cl⁻ can be detected by 0.1 M AgNO₃. The filter cakes were grounded and sieved through 80 mesh screen after dried at constant temperature for 24 h. The obtained samples were calcinated for 3 h at 110, 250, 400, 500, 600 and 700 °C, respectively.

To investigate the influence of Fe³⁺ doping on the phase transformation, crystal growth kinetics, the pure titanium hydroxide was prepared according to the same procedure as the above mentioned except the dripping of Fe(NO₃)₃ solution.

Characterization: Thermal decomposition analysis was performed on a shimadzu DT-30 thermal analyzer under the protection of nitrogen gas flow. The heating rate was 10 K min⁻¹.

X-ray powder diffraction patterns were obtained at room temperature by a Philips diffractometer model XPert MPD using CuK α radiation at scanning step 0.02° and scanning rate 1°/min PC-APD 4.0 software was used to separate K α_2 from K α_1 . The whole X-ray pattern was fitted by GSAS (general structure analysis system)¹³, a free software created by Larson and Von Dreele of American Los Alamos National Laboratory for the Rietveld refinement of structural models to both X-ray and neutron

diffraction data. The grain size and lattice strain were calculated according to eqns. 1 and 2.

$$P = \frac{18000K\lambda}{\pi x} \quad (1) \quad S = \frac{\pi}{18000}(Y - Y_i) \times 100 \% \quad (2)$$

where K is the Scherrer constant; X and Y are the peak profile refinement parameters LX and LY, respectively; Y_i is the profile parameter of reference sample without micro-strain. The units are Å.

RESULTS AND DISCUSSION

TG/DTA analysis: Fig. 1 shows the TG-DTA curve for pure titanium hydrate, co-precipitation Fe³⁺-doped (0.5 %) titanium hydrate and step-precipitation Fe³⁺-doped titanium hydrate prepared by TiCl₄ hydrolyzation. An endothermal peak appears near 373 K on all three curves due to the desorption of adsorbed water. The corresponding TG curves also show an obvious weight loss. The amount of adsorbed water can be calculated from the area of these endothermal peaks. The mass losses for pure titanium hydrate, co-precipitation Fe³⁺-doped titanium hydrate and step-precipitation Fe³⁺-doped titanium hydrate are 16.3, 27.5 and 25.6 %, respectively. The significant differences indicate the different constitution of three samples. The theoretical mass losses of TiO₂·2H₂O and TiO₂·H₂O are 31.0 and 18.3 %. Therefore pure titanium hydrate is supposed to exist in the form of TiO₂·H₂O while Fe³⁺-doped titanium hydrate in the form of TiO₂·xH₂O (x = 1-2).

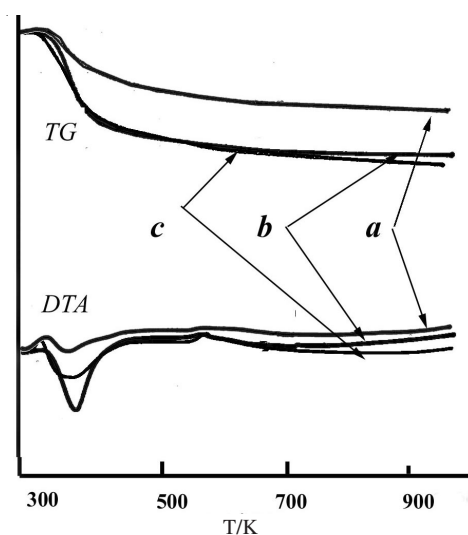


Fig. 1. TG and DTA curves for (a) pure titanium hydroxide and 0.5 % of Fe³⁺-doped titanium hydroxide prepared by (b) co-precipitation (c) step precipitation

XRD analysis of TiO₂ ultrafine powder treated at different calcinating temperature: Fig. 2(A)-(C) show the XRD patterns of pure TiO₂, co-precipitation 0.5 %

Fe^{3+} -doped TiO_2 powder and step-precipitation Fe^{3+} -doped TiO_2 powder calcinated at different temperatures for 3 h. From the figures, the original powders prepared by TiCl_4 hydrolyzation are amorphous. With the increase of calcinating temperature, amorphous TiO_2 gradually transforms to anatase. The diffraction peak characteristic of anatase intensifies. No obvious exothermal peaks were detected above 500 K for pure titanium hydrate in that we suppose that crystallization process from amorphous to anatase takes place gradually among the whole temperature range. This is not consistent with the commonly reported the existence of crystallization temperature for amorphous titanium dioxide. But as to Fe^{3+} -doped titanium hydrate, a weak exothermal peak appears near 650 K on DTA curve possibly because the Fe^{3+} doping facilitates the transformation from amorphous phase to anatase and speeds up the heat liberation in the process of crystallization. From Fig. 2, Fe^{3+} doping, especially in step-precipitation sample, prompts the phase transformation from anatase to rutile.

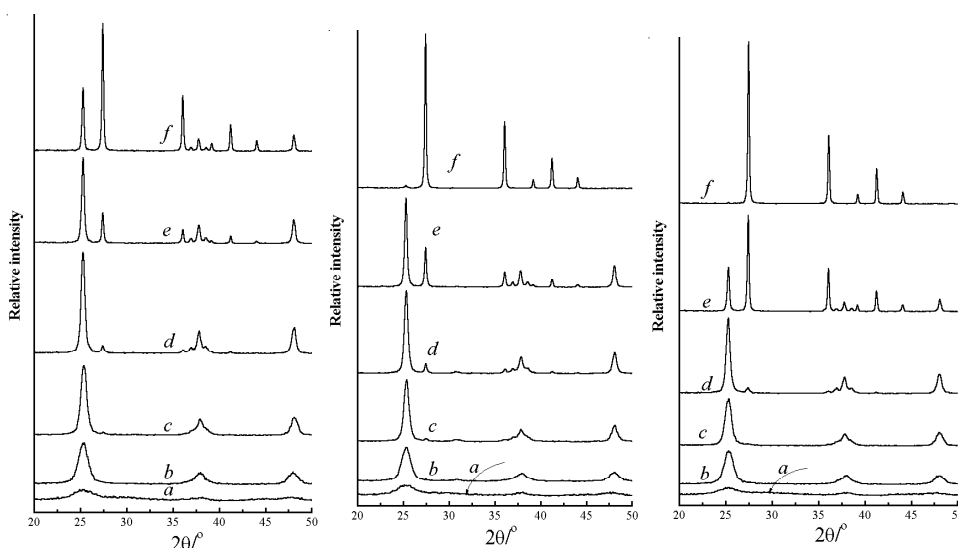


Fig. 2. XRD pattern of pure titanium dioxide prepared (A), co-precipitation Fe^{3+} -doped titanium dioxide (B) and step-precipitation Fe^{3+} -doped titanium dioxide (C) prepared by TiCl_4 hydrolyzation calcinated at (a) 110 °C (b) 250 °C (c) 400 °C (d) 500 °C (e) 600 °C (f) 700 °C for 3 h

Micro-structure parameter and growth kinetics of TiO_2 ultrafine powder:

To obtain such structural parameters as exact cell parameter, grain size, lattice parameter, *etc.* of pure and Fe^{3+} -doped titanium dioxide, Rietveld refinement software GSAS (general structure analysis system) is used here. Parameters including cell parameters, atomic coordination, UISO, background, scaling, profile parameters GU, GV, GW, LX, LY, S/L, H/L, *trans*, *shft*, preferential orientation are refined. Appropriate refinement sequence is selected and after some cycles of refinement,

the convergence is achieved. The ultimate Rietveld refinement results of step-precipitation Fe³⁺-doped titanium hydrate calcinated at 600 °C for 3 h is shown in Fig. 3. The calculated pattern matches the observed pattern well. All refined results are listed in Table-1.

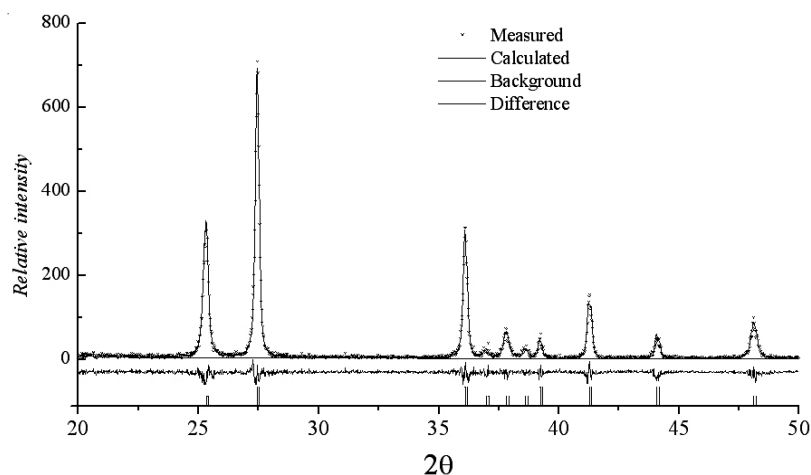


Fig. 3. Ultimate Rietveld refinement results of step-precipitation Fe³⁺-doped titanium hydrate calcinated at 600 °C for 3 h. The calculated pattern matches the observed pattern well

When Fe³⁺-doped titanium dioxide is calcinated for a certain period of time, Fe³⁺ can possibly exist in two positions. First, it can occupy the position of Ti⁴⁺. The ionic radius of Fe³⁺ is 0.064 nm, which is close to the radius of Ti⁴⁺ 0.068 nm. Thus Fe³⁺ is relatively easy to penetrate into the Ti⁴⁺ position. We can see from the Table-1 that the cell parameters of pure TiO₂ and Fe³⁺-doped TiO₂ are close to each other and that with the increase of calcinating temperature, more and more amount of Fe³⁺ penetrates into the crystal lattice, but there is little change in cell parameters. On the other hand, because of the differences in valence and coordination number, some kind of distortion does exist in the case of Fe³⁺ replacement. For example, when calcinating temperature increases, both co-precipitation and step-precipitation Fe³⁺-doped TiO₂ exhibit increasing micro-strain. This strain must be released before phase transformation can take place. So, the micro-strain gradually decreases when phase transformation from anatase to rutile starts above calcinating temperature 500 °C and it accumulates again in the newly formed rutile phase. Therefore, the substitution of Fe³⁺ instead of Ti⁴⁺ is an unfavorable factor in facilitating phase transformation. Second, Fe³⁺ serves as a interstitial atom and is reduced according to equation $2M^{n+} + O^{2-} \rightarrow 2M^{(n-1)+} + 1/2O_2 + Va$. In the equation, Va is an oxygen vacancy, which is supposed to be the main factor promoting the A-R phase transformation of TiO₂¹⁴. In the case of co-precipitating, Fe³⁺ mixed evenly with the hydrolyzing Ti⁴⁺ and has a better chance to occupy the position of Ti⁴⁺ while in the case of

TABLE-1
RESULTS OF RIETVELD REFINEMENT BY GENERAL
STRUCTURE ANALYSIS SYSTEM (GSAS)

Temperature °C step-precipitation		Cell parameter Å			D	e (%)	Phase content (%)		
		a	b	c	nm				
Step-precipitation	250	Anatase	3.777	3.777	9.462	8.7	0	100	
		Rutile	–	–	–	–	–	0	
	400	Anatase	3.785	3.785	9.504	15.1	0.36	100	
		Rutile	–	–	–	–	–	0	
	500	Anatase	3.785	3.785	9.511	25.2	0.28	92.4	
		Rutile	4.594	4.594	2.963	30.5	0	7.6	
	600	Anatase	3.780	3.780	9.506	73.6	0.19	14.7	
		Rutile	4.590	4.590	2.957	150.0	0.25	85.3	
	700	Anatase	–	–	–	–	–	0	
		Rutile	4.584	4.584	2.955	650	0.37	100	
	Co-precipitation	250	Anatase	3.778	3.778	9.462	12.1	0	100
			Rutile	–	–	–	–	–	0
400		Anatase	3.782	3.782	9.504	13.9	0.45	100	
		Rutile	–	–	–	–	–	0	
500		Anatase	3.785	3.785	9.508	20.3	0.40	93.2	
		Rutile	4.596	4.596	2.967	26.6	0	6.8	
600		Anatase	3.782	3.782	9.506	50.6	0.23	70.6	
		Rutile	4.592	4.592	2.958	125.2	0.32	29.4	
700		Anatase	3.782	3.782	9.505	144.0	0.20	3.6	
		Rutile	4.583	4.583	2.955	521.5	0.40	96.4	
Pure titanium dioxide		250	Anatase	3.776	3.776	9.460	13.8	0	100
			Rutile	–	–	–	–	–	0
	400	Anatase	3.780	3.780	9.469	14.6	0.23	100	
		Rutile	–	–	–	–	–	0	
	500	Anatase	3.783	3.783	9.508	22.7	0.18	94.8	
		Rutile	4.593	4.593	2.963	28.9	0	5.2	
	600	Anatase	3.780	3.780	9.505	80.2	0.15	80.5	
		Rutile	4.588	4.588	2.956	139.4	0.19	19.5	
	700	Anatase	3.780	3.780	9.503	250.3	0.15	21.3	
		Rutile	4.582	4.582	2.953	596.8	0.28	78.7	

step-precipitation, Fe^{3+} is adsorbed on the interface of micro-crystal titanium hydrate and is more likely to serve as interstitial atoms. Therefore, Fe^{3+} doping, especially step-precipitation, favors the A-R phase transformation of titanium dioxide and it can be easily concluded according the phase content listed in the Table-1.

Crystallite size for both pure TiO_2 and Fe^{3+} -doped TiO_2 increases with the increasing temperature. Before transformation occurs, crystal grows slowly. Grain size varies between 20-30 nm below 500 °C. Micro-crystal grows quickly when phase transformation starts. From the Table-1 at the same calcinating temperature, the crystallite size increases in the order of co-precipitation TiO_2 has the smallest grain size, followed by step-precipitation and pure TiO_2 . The activation energy of crystal

growth can be calculated according to the sizes at different calcinating temperature. From the theory of phase transformation, the nuclei growth speed during crystallization of amorphous substances is as follows¹⁵:

$$u = c [\exp(-Q/RT)][1-\exp(-Fv/kT)] \quad (3)$$

In the formula, u is nuclei growth speed; c is a constant; Fv is mole free energy difference between crystal and amorphous material; Q is the nuclei growth activation energy. Generally, the degree of super-cooling for amorphous solid is high. Therefore, the driving force of phase transformation Fv is much larger than kT . The formula 3 can be simplified as

$$u = c [\exp(-Q/kT)] \quad (4)$$

Here nuclei are supposed to grow at constant speed and the grain size is proportional to u . The relationship between $\ln u$ and $1/T$ is revealed in Fig. 4. The crystal growth of Fe³⁺-doped and pure TiO₂ can be divided into two obvious stages with the turning point at phase transformation temperature. In the case of pure TiO₂, the crystal growth activation energy is calculated to be $Q_1 = 1.5$ and $Q_2 = 74.2$ kJ/mol. In the case of co-precipitation Fe³⁺-doped TiO₂, $Q_1 = 2.9$ and $Q_2 = 60.8$ kJ/mol. As to step-precipitation Fe³⁺-doped TiO₂, there is no obvious turning point because of complete phase transformation before 550 °C. Its overall activation energy is about 23.1 kJ/mol. The obvious differences in activation energy between the two stages may be related to the swallow mechanism of crystallite growth where bigger grains "swallow" small particles. Only anatase grain exists below 500 °C. When calcinating temperature is above 500 °C, on one hand, bigger grains continue to "swallow" small particles to grow, therefore small grains become fewer. On the other hand, as A-R phase transformation continues, more anatase grains transform to rutile. From the thermodynamics point of view, the transformation of anatase to rutile is irreversible. Thus small anatase grains supplements for big grains to grow are fewer and fewer. Anatase grain growth becomes difficult and apparent activation energy increases greatly.

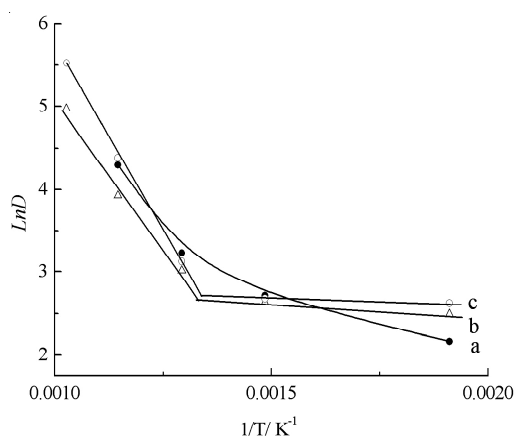


Fig. 4. $\ln D$ versus $1/T$ for (a) step-precipitation Fe³⁺-doped TiO₂; (b) co-precipitation Fe³⁺-doped TiO₂; (c) pure TiO₂

TEM image for Fe³⁺-doped TiO₂ ultrafine powder: TEM images for pure and Fe³⁺-doped TiO₂ prepared by TiCl₄ step-precipitation and co-precipitation hydrolyzation, calcinated at 400 °C for 3 h are shown in Fig. 5. From the figures, it seems that large particles about 1-2 μm with irregular shape are composed of small sized particles about 20-30 nm. Those small grains can be observed clearly on the edge of the large agglomerations. The grain size obtained here is in good agreement with Rietveld refinements.

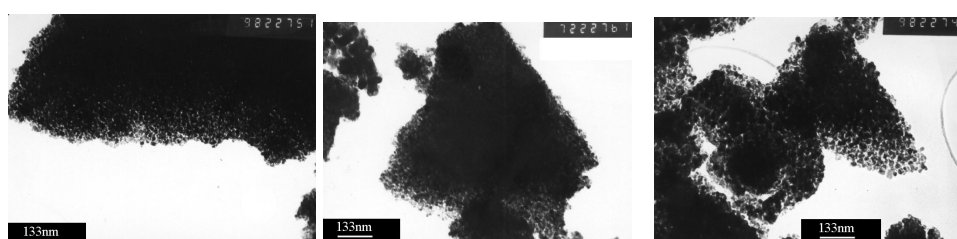


Fig. 5. TEM image of pure titanium dioxide prepared (A), co-precipitation Fe³⁺-doped titanium dioxide (B) and step-precipitation Fe³⁺-doped titanium dioxide (C) prepared by TiCl₄ hydrolyzation calcinated at 400 °C for 3h

Conclusion

Pure TiO₂, co-precipitation Fe³⁺-doped TiO₂ and step-precipitation Fe³⁺-doped TiO₂ are synthesized by the method of TiCl₄ hydrolyzation. Fe³⁺ doping, especially step-precipitation sample, prompts the phase transformation from anatase to rutile. Cell parameters, micro-strain, grain size and phase content are calculated by rietveld refinement. They change regularly with the variation of calcinating temperature. The results show that the Fe³⁺ doping influences the phase transformation of titanium dioxide in two ways, *i.e.*, the substitution of Fe³⁺ instead of Ti⁴⁺ and the creation of oxygen vacancy by interstitial Fe³⁺ reaction. Studies on anatase grain growth kinetics show that it can be divided into two obvious stages with the turning point at phase transformation temperature. In the case of pure TiO₂, the crystal growth activation energy is calculated to be Q1 = 1.5 and Q2 = 74.2 kJ/mol. In the case of co-precipitation Fe³⁺-doped TiO₂, Q1 = 2.9 and Q2 = 60.8 kJ/mol. As to step-precipitation Fe³⁺-doped TiO₂, there is no obvious turning point because of complete phase transformation before 550 °C. The overall activation energy is about 23.1 kJ/mol.

ACKNOWLEDGEMENTS

The authors gratefully acknowledge support for this work from Zhejiang Natural Science Foundation (Grant No. Y407058), Ningbo Science & Technology Bureau project (Grant No. 2006B100064, 2008A610060) and K.C. Wong Magna Fund in Ningbo University.

REFERENCES

1. K.I. Hadjiivanov and D.G. Klissurski, *Chem. Soc. Rev.*, **25**, 61 (1996).
2. A. Maldoti, A. Molinari and R. Amadeni, *Chem. Rev.*, **102**, 3811 (2002).
3. E. Haro-Paniatowski, R. Rodriguex-Talavera, M. Heredia de la Cruz, O. Cano-Corona and R. Arroyo-Murillo, *J. Mater. Res.*, **9**, 2102 (1994).
4. L.D. Birkefeld, M.A. Adal and S.A. Akbor, *J. Am. Ceram. Soc.*, **75**, 2964 (1992).
5. M. Gratzel, *Nature*, **414**, 338 (2001).
6. M. Adachi, *J. Am. Chem. Soc.*, **126**, 14943 (2004).
7. S. Zhang, L.M. Peng, Q. Chen, G.H. Du, G. Dawson and W.Z. Zhou, *Phys. Rev. Lett.*, **91**, 256103 (2003).
8. S. Doeff, M. Henry, C. Sanchez and J. Livage, *J. Non-Crystalline Solid*, **89**, 206 (1987).
9. W. Wang, B. Gu, L. Liang, W.A. Hamilton and D.J. Wesolowski, *J. Phys. Chem. B*, **108**, 39 (2004).
10. D. Mardare, F. Iacomi and D. Luca, *Thin Solid Films*, **515**, 6474 (2007).
11. W. Zhang, Y. Li, S. Zhu and F. Wang, *Chem. Phys. Lett.*, **373**, 333 (2003).
12. S.K. Hazra and S. Basu, *Sens. Actuators B*, **115**, 403 (2006).
13. A.C. Larson and R.B. Von Dreele, GSAS Manual, Los Alamos National Laboratory Report LAUR pp. 86-748 (2004).
14. K.L.D. Mackenzie, *Trans. J. Br. Ceram. Soc.*, **74**, 121 (1975).
15. M.G. Scott, in ed.: F. E. Luboraky, *Amorphous Metallic Alloys*, Butterworths Co. Ltd., London, pp. 151-159 (1983).

(Received: 13 June 2009; Accepted: 16 January 2010) AJC-8307

**22ND INTERNATIONAL CONFERENCE ON
INDIUM PHOSPHIDE AND RELATED MATERIALS (IPRM'10)**

31 MAY — 4 JUNE 2010

KAGAWA, JAPAN

Contact:

IPRM2010 Secretariat, C/o Event and Convention House,
Inc., 8F Shuwa-Okachimachi Bldg., 4-27-5 Taito,
Taito-ku, Tokyo 110-0016 Japan
Tel: +81-3-3831-2601, Fax: +81-3-5807-3019,
E-mail: iprm2010@ech.co.jp
Web site: http://www.iprm.jp/html/iprm_top.html